

# A SPACE-TIME HYBRID PARAREAL METHOD FOR KINETIC EQUATIONS IN THE DIFFUSIVE SCALING

TINO LAIDIN

**ABSTRACT.** We present a novel multiscale numerical approach that combines parallel-in-time computation with hybrid domain adaptation for linear collisional kinetic equations in the diffusive regime. The method addresses the computational challenges of kinetic simulations by integrating two complementary strategies: a parareal temporal parallelization method and a dynamic spatial domain adaptation based on perturbative analysis. The parallel in time approach employs a coarse fluid solver for efficient temporal propagation coupled with a fine, spatially-hybridized, kinetic solver for accurate resolution. Domain adaptation is governed by two criteria: one measuring the deviation from local velocity equilibrium, and another based on macroscopic quantities available throughout the computational domain. An asymptotic preserving micro-macro decomposition framework handles the stiffness of the original problem. This fully hybrid methodology significantly reduces computational costs compared to full kinetic approaches by exploiting the lower dimensionality of asymptotic fluid models while maintaining accuracy through selective kinetic resolution. The method demonstrates substantial speedup capabilities and efficiency gains across various kinetic regimes.

2020 MATHEMATICS SUBJECT CLASSIFICATION: *Primary*: 35Q20, 65M22, 82C40, *Secondary*: 65M55, 65Y05.

## 1. INTRODUCTION

The numerical simulation of kinetic equations is a longstanding challenge due to their high dimensionality and the presence of multiple scales. A prototypical example is the Vlasov–Poisson system with linear BGK collisions, which arises in collisional plasma physics and semiconductor modeling. The unknown is the distribution function  $f(t, x, v)$  depending on time  $t \geq 0$ , position  $x \in \mathbb{T}^{d_x}$  the  $d_x$ -dimensional torus, and velocity  $v \in \mathbb{R}^{d_v}$ . It describes the probability of observing a particle at time  $t$  and position  $x$  moving at velocity  $v$ . In the *diffusive scaling*, the model reads

$$\begin{cases} \varepsilon \partial_t f + v \cdot \nabla_x f + E \cdot \nabla_v f = \frac{1}{\varepsilon} \mathcal{Q}(f), \\ f(0, x, v) = f_{\text{in}}(x, v), \end{cases} \quad (\mathcal{P}^\varepsilon)$$

where  $\varepsilon > 0$  is the Knudsen number,  $E = -\nabla_x \phi$  is the self-consistent electric field, and  $\mathcal{Q}(f) = \rho \mathcal{M} - f$  is the linear BGK operator driving relaxation toward a local equilibrium. Here  $\rho = \langle f \rangle = \int_{\mathbb{R}^{d_v}} f \, d v$  denotes the macroscopic density, and the Maxwellian is defined by

$$\mathcal{M}(v) = \frac{1}{(2\pi)^{d_v/2}} \exp\left(\frac{|v|^2}{2}\right). \quad (1)$$

The Poisson equation closes the system:

$$\Delta \phi^\varepsilon = \rho^\varepsilon - \bar{\rho} \quad \text{with} \quad \bar{\rho} = \iint f_{\text{in}} \, d x \, d v. \quad (2)$$

The collision operator conserves mass, i.e.

$$\int_{\mathbb{R}^{d_v}} \mathcal{Q}(f) \, d v = 0, \quad (3)$$

so that the total number of particles is preserved.

---

(Tino Laidin) UNIV BREST, CNRS UMR 6205, LABORATOIRE DE MATHÉMATIQUES DE BRETAGNE ATLANTIQUE, F-29200 BREST, FRANCE

*E-mail address:* tino.laidin@univ-brest.fr.

*Key words and phrases.* Kinetic equations, micro–macro decomposition, parareal, domain adaptation, multiscale methods,

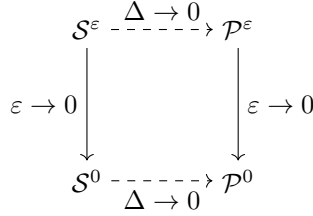


FIGURE 1. Asymptotic-Preserving diagram

The Knudsen number, defined as the ratio between the mean free path of particles and a characteristic length, quantifies the importance of collisions and determines the current regime. When  $\varepsilon \sim 1$ , transport dominates and only few collisions occur: this is the kinetic regime. Conversely, when  $\varepsilon \ll 1$ , collisions dominate and the system rapidly approaches a local Maxwellian equilibrium. In this fluid regime, macroscopic quantities drive the dynamics. In the diffusive scaling [10], the macroscopic density  $\rho^\varepsilon$  converges towards a limit  $\rho$  solution to a drift–diffusion system

$$\begin{cases} \partial_t \rho(t, x) - \nabla_x \cdot J(t, x) = 0, & J(t, x) = \nabla_x \rho(t, x) - E(t, x)\rho(t, x), \\ \rho(0, x) = \rho_{\text{in}}(x), \end{cases} \quad (\mathcal{P}^0)$$

with  $E$  determined by the Poisson equation (2).

From the computational viewpoint, equation  $(\mathcal{P}^\varepsilon)$  suffers from two intrinsic difficulties. First, the distribution function depends on both position and velocity, leading to the curse of dimensionality. In general, the phase space is six-dimensional, making grid-based methods very costly. Second, the stiff relaxation term  $(1/\varepsilon)\mathcal{Q}(f)$  imposes severe constraints of the form  $\Delta t \leq \varepsilon \Delta x$  on explicit time discretizations. These challenges motivated the development of *Asymptotic-Preserving* (AP) schemes, which remove the stiffness barrier by capturing the asymptotic limit uniformly in  $\varepsilon$  [32, 30, 14, 31]. As shown in Figure 1, the AP property ensures that  $S^\varepsilon$  converges to  $S^0$  as  $\varepsilon \rightarrow 0$ , with  $S^0$  recovering the solution to the asymptotic model in the limit of vanishing discretization parameters. While AP schemes allow time steps independent of  $\varepsilon$ , they remain globally kinetic and thus computationally demanding, even in fluid regimes where the dynamics should be cheap to compute.

To reduce the numerical cost, various *hybrid kinetic–fluid methods* have been proposed. The general idea is to exploit the validity of fluid approximations near local equilibrium, restricting kinetic solvers to localized non-equilibrium subdomains. This reduces complexity by leveraging lower-dimensional macroscopic solvers in large regions of the domain. A key challenge is to design reliable criteria to decompose the domain into kinetic and fluid parts, using either macroscopic indicators or measures of the distance from equilibrium [48, 50, 9, 33]. In this work, we adopt the approach introduced in [41, 49, 23, 24] under the hydrodynamic scaling, and later extended to the diffusive scaling in [34, 36]. The main idea is to rely on two criteria derived from a perturbative analysis. First, a hierarchy of macroscopic models is constructed through the Chapman–Enskog expansion of the distribution function, leading to a moment realizability criterion that quantifies the deviation of kinetic moment dynamics from their fluid counterparts. Second, the magnitude of the perturbation is used to measure the deviation from the Maxwellian equilibrium. These dynamic domain adaptation methods are typically applied cell-wise in time, although their efficiency may be reduced when kinetic regions remain spatially extended.

Other strategies have been explored, such as buffer zones with smooth transition functions [11, 9, 12] within the continuous model, or velocity-space hybridization based on a Maxwellian–perturbation decomposition [13, 6, 28, 29]. While these methods provide substantial savings, their benefits also remain limited in highly kinetic regimes.

In parallel, *parallel-in-time algorithms* such as the parareal [42, 43] and the MultiGrid Reduction In Time (MGRIT) [21, 15] methods have emerged as powerful tools to accelerate time integration of dynamical systems. The parareal method combines a coarse, inexpensive propagator with a fine, accurate solver, iteratively correcting the coarse prediction in parallel, while MGRIT extends this idea to a multilevel framework. These methods are known to

converge rapidly for diffusion-dominated problems but also to face significant difficulties in advection-dominated dynamics [22, 3, 25, 20, 45, 2, 27, 47, 8]. The kinetic regime therefore appears particularly challenging. Nevertheless, given the high cost of kinetic simulations, even slowly converging parallel-in-time algorithms can provide substantial computational savings. Conversely, since the asymptotic limit ( $\mathcal{P}^0$ ) of ( $\mathcal{P}^\varepsilon$ ) is diffusive, good convergence can be expected in this regime. The application of the parareal method to multiscale problems has received particular attention [17, 38, 26, 46, 4], where coarse propagators are constructed from reduced asymptotic models. In addition, recent works [44, 37] emphasize that coarse propagation within the parareal method need not be restricted to temporal coarsening, but can instead involve coarser spatial grids or dimension reduction, a perspective particularly relevant for kinetic equations. These strategies naturally connects with the Heterogeneous Multiscale Method (HMM) framework [19, 18, 1].

Building on these ideas, a kinetic–fluid parareal method was recently introduced in [37]. In this setting, the fluid, hyperbolic model provides the coarse solver, while the kinetic solver captures fine-scale effects. In this scaling, efficiency is delicate. The combination of hyperbolic (presence of shocks) and kinetic (transport-dominated) solvers can hinder convergence. In our setting, applying a diffusive scaling eliminates the challenges of the hyperbolic limit, replacing them with a dynamics more parareal-compatible.

The present work introduces a novel space–time multiscale numerical methodology that combines three ingredients namely AP schemes, hybridization in space, and parallel-in-time acceleration into a unified framework for the Vlasov–Poisson–BGK system in the diffusive scaling. The key components are:

- an *asymptotic-preserving micro–macro scheme* that handles stiffness and ensures consistency with the diffusion limit;
- a *hybrid kinetic–fluid phase-space solver*, dynamically adapting the computational domain based on deviation from local equilibrium and macroscopic indicators;
- a *multiscale parallel-in-time strategy*, coupling the fluid solver as a coarse propagator with the above hybrid solver as the fine propagator via the parareal algorithm.

This combination leverages the robustness of AP schemes in stiff regimes, the dimensional reduction of hybrid solvers, and the scalability of the parareal algorithm. The resulting method yields significant computational savings compared to an AP, but fully kinetic approach, while preserving accuracy across both kinetic and fluid regimes.

The paper is organized as follows. Section 2 recalls the dynamic domain adaptation and numerical schemes. Section 3 presents the parallel-in-time algorithm and its coupling with the hybrid solver, leading to a space–time hybrid solver. The implementation of the method is briefly discussed in Section 4 and section 5 presents numerical experiments illustrating the efficiency and accuracy of the method.

## 2. DYNAMIC DOMAIN ADAPTATION

In this section, we recall the building blocks of the dynamic domain adaptation introduced in [34, 36] for kinetic equations in the diffusive scaling. We start by presenting a hierarchy of macroscopic models used to define coupling criteria and then present the numerical schemes used.

**2.1. Macroscopic hierarchy.** To obtain a macroscopic coupling criterion, a hierarchy of macroscopic models is built from an asymptotic expansion of the distribution. We introduce the truncated Chapman-Enskog expansion of  $f^\varepsilon$  at order  $L \in \mathbb{N}$ :

$$f^\varepsilon(t, x, v) = \rho^\varepsilon(t, x)\mathcal{M}(v) + \sum_{l=1}^L \varepsilon^l h^{(l)}(t, x, v). \quad (4)$$

By inserting (4) into the original equation ( $\mathcal{P}^\varepsilon$ ), one can identify powers of epsilon to obtain

$$l = 0 : \quad h^{(1)} = -\mathbf{T}(\rho^\varepsilon \mathcal{M}), \quad (5a)$$

$$l = 1 : \quad h^{(2)} = -\partial_t(\rho^\varepsilon \mathcal{M}) - \mathbf{T}(h^{(1)}), \quad (5b)$$

$$2 \leq k \leq L-1 : \quad h^{(l+1)} = -\partial_t h^{(l-1)} - \mathbf{T}(h^{(l)}), \quad (5c)$$

Derivative \ Index	-3	-2	-1	0	1	2	3
1	-1/60	3/20	-3/4	0	3/4	-3/20	1/60
2	1/90	-3/20	3/2	-49/18	3/2	-3/20	1/90
3	1/8	-1	13/8	0	-13/8	1	-1/8
4	-1/6	2	-13/2	28/3	-13/2	2	-1/6

TABLE 1. Central finite differences coefficients.

where  $\mathsf{T}f = v \cdot \nabla_x f + E \cdot \nabla_v f$  is the transport operator. The hierarchy of macroscopic models is obtained by truncation of (4) plugged into  $(\mathcal{P}^\varepsilon)$  and integrated in velocity. Note that the first order allows us to formally recover the asymptotic model  $(\mathcal{P}^0)$ .

Let us now recall the macroscopic model obtained by setting  $L = 3$ . In the  $d_x = 1$  and  $d_v = 3$  setting, it was shown in [36, Section 2] that the higher order macroscopic model writes

$$\partial_t \rho^\varepsilon - \partial_x J^\varepsilon = -\varepsilon^2 \mathcal{R} + \mathcal{O}(\varepsilon^4), \quad (6)$$

where the remainder  $\mathcal{R}^\varepsilon$  is given by

$$\mathcal{R}^\varepsilon = -\partial_{xxx} J^\varepsilon + E \partial_{xx} J^\varepsilon + (2\rho^\varepsilon - 3\bar{\rho}) \partial_x J^\varepsilon + 2J^\varepsilon \partial_x \rho^\varepsilon - \partial_x \rho^\varepsilon \partial_t E^\varepsilon. \quad (7)$$

In the following, the  $d_x = 1$  and  $d_v = 3$  will be considered and extensions of (6) to higher dimensions are discussed in [35, Appendix A].

**2.2. Domain indicators.** The idea of the dynamic domain decomposition is to approximate the kinetic system by its fluid counterpart whenever possible, thereby exploiting the reduced computational cost of fluid solvers. To ensure accuracy, the domain partition must dynamically track the local state of the solution. At each time step, the status of each spatial cell is updated according to two coupling thresholds,  $\delta_0$  and  $\eta_0$ , defined through the following indicators:

- If  $|\mathcal{R}^\varepsilon| < \delta_0$ , then the dynamic of the solution to (6) is sufficiently close to the one of limit model  $(\mathcal{P}^0)$ , and the fluid description can be employed;
- Let  $g = f - \rho\mathcal{M}$ . If  $\|g^\varepsilon\| < \eta_0$ , the solution is close to local equilibrium in velocity space, and again the fluid description is admissible.

If neither condition is satisfied, the corresponding cell remains (or switches to) kinetic. In practice, the thresholds  $\delta_0$  and  $\eta_0$  are chosen to balance accuracy and efficiency: too large values may trigger the fluid approximation prematurely, while too small values may reduce computational gains. Furthermore, as  $\mathcal{R}^\varepsilon$  involves high-order derivatives, the finite differences presented in Table 1 are used for its approximation in each cell. Regarding the computation of the criterion on the perturbation, a classical  $L^2$ -norm is used.

**2.3. Numerical schemes. Mesh and discretization.** We restrict ourselves to the case  $d_x = 1$  and  $d_v = 3$  used in the numerical experiments. Let  $\mathcal{I} = \{1, \dots, N_x\}$  and  $\mathcal{J} = \{1, \dots, N_v\}$ . The  $(x, v)$ -phase space is discretized in a finite-volume fashion with control volumes  $K_{ij} = \mathcal{X}_i \otimes \mathcal{V}_j$ , for  $i \in \mathcal{I}$  and  $j = (j_x, j_y, j_z) \in \mathcal{J}^3$ . We denote by  $\Delta x$  and  $\Delta v^3$  the uniform volumes of  $\mathcal{X}_i$  and  $\mathcal{V}_j$  respectively.

**Micro–macro scheme.** Following [34, 36], we use a finite volume relaxed AP micro–macro scheme introduced in [40, 39, 7], based on the decomposition

$$f(t, x, v) = \rho(t, x)\mathcal{M}(v) + g(t, x, v), \quad (8)$$

where  $g$  is the perturbation from the Maxwellian. The resulting scheme writes

$$\begin{cases} g_{i+\frac{1}{2},j}^{\varepsilon,n+1} = g_{i+\frac{1}{2},j}^{\varepsilon,n} e^{-\Delta t/\varepsilon^2} - \varepsilon(1 - e^{-\Delta t/\varepsilon^2}) \left( \frac{T_{i+\frac{1}{2},j}^{\varepsilon,n}}{\Delta x \Delta v^3} + \xi_j \mathcal{M}_j J_{i+\frac{1}{2}}^{\varepsilon,n} \right), \\ \rho_i^{\varepsilon,n+1} = \rho_i^{\varepsilon,n} - \frac{\Delta t}{\varepsilon \Delta x} \left( \langle \xi g_{i+\frac{1}{2}}^{\varepsilon,n+1} \rangle_\Delta - \langle \xi g_{i-\frac{1}{2}}^{\varepsilon,n+1} \rangle_\Delta \right), \\ E_{i+\frac{1}{2}}^{\varepsilon,n} - E_{i-\frac{1}{2}}^{\varepsilon,n} = (\rho_i^{\varepsilon,n} - \bar{\rho}) \Delta x, \end{cases} \quad (\mathcal{S}^{\text{MM}})$$

where  $\xi_j$  denotes the  $x$ -component of  $v_j$ , and  $T_{i+\frac{1}{2},j}^{\varepsilon,n}$  is an upwind discretization of the transport term  $\mathbf{T}g - \partial_x \langle v_x g \rangle \mathcal{M}$ . For fixed  $\Delta x, \Delta v > 0$ , the scheme is AP in the diffusion limit, independently of the initial data [34].

**Limit scheme.** As  $\varepsilon \rightarrow 0$ , one recovers a discretization of  $(\mathcal{P}^0)$ :

$$\begin{cases} \rho_i^{n+1} = \rho_i^n + m_2^{\Delta v} \frac{\Delta t}{\Delta x} \left( J_{i+\frac{1}{2}}^n - J_{i-\frac{1}{2}}^n \right), \\ J_{i+\frac{1}{2}}^n = \frac{\rho_{i+1}^n - \rho_i^n}{\Delta x} - E_{i+\frac{1}{2}} \rho_{i+\frac{1}{2}}^n, \quad E_{i+\frac{1}{2}}^n - E_{i-\frac{1}{2}}^n = (\rho_i^n - \bar{\rho}) \Delta x, \end{cases} \quad (\mathcal{S}^0)$$

with  $m_2^{\Delta v} = \sum_{l \in \mathcal{J}} v_l^2 M_l \Delta v_l$ .

**Hybrid scheme.** Combining  $(\mathcal{S}^{\text{MM}})$  and  $(\mathcal{S}^0)$  then yields the hybrid micro-macro scheme. The AP scheme  $(\mathcal{S}^{\text{MM}})$  is applied in kinetic cells within  $\Omega_{\mathcal{K}}$ , while the limit scheme  $(\mathcal{S}^0)$  is used in cells of  $\Omega_{\mathcal{F}}$ .

$$\begin{cases} g_{i+\frac{1}{2},j}^{\varepsilon,n+1} = g_{i+\frac{1}{2},j}^{\varepsilon,n} e^{-\Delta t/\varepsilon^2} - \varepsilon \left( 1 - e^{-\Delta t/\varepsilon^2} \right) \left( \frac{T_{i+\frac{1}{2},j}^{\varepsilon,n}}{\Delta x \Delta v^3} + \xi_j M_j J_{i+\frac{1}{2}}^{\varepsilon,n} \right), \quad \mathcal{X}_{i+\frac{1}{2}} \in \Omega_{\mathcal{K}}^n, \\ g_{i+\frac{1}{2},j}^{\varepsilon,n+1} = 0, \quad \mathcal{X}_{i+\frac{1}{2}} \in \Omega_{\mathcal{F}}^n, \\ \rho_i^{\varepsilon,n+1} = \rho_i^{\varepsilon,n} + \frac{\Delta t}{\Delta x} \tilde{J}_i^{\varepsilon,n}, \\ \tilde{J}_i^{\varepsilon,n} = \begin{cases} -\frac{1}{\varepsilon} (\langle \xi g_{i+\frac{1}{2}}^{\varepsilon,n+1} \rangle_{\Delta} - \langle \xi g_{i-\frac{1}{2}}^{\varepsilon,n+1} \rangle_{\Delta}), & \mathcal{X}_i \in \Omega_{\mathcal{K}}^n, \\ m_2^{\Delta v} (J_{i+\frac{1}{2}}^n - J_{i-\frac{1}{2}}^n), & \mathcal{X}_i \in \Omega_{\mathcal{F}}^n, \end{cases} \\ E_{i+\frac{1}{2}}^{\varepsilon,n} - E_{i-\frac{1}{2}}^{\varepsilon,n} = (\rho_i^{\varepsilon,n} - \bar{\rho}) \Delta x. \end{cases} \quad (\mathcal{S}^{\text{HMM}})$$

with the update of  $\Omega_{\mathcal{K}}^n$  and  $\Omega_{\mathcal{F}}^n$  detailed in Section 2.2. Note that the perturbation  $g$  is set to 0 in  $\Omega_{\mathcal{F}}$ , corresponding to the assumption that the solution is exactly at equilibrium. A finer treatment would replace  $g$  by its expansion in (4), which can be computationally expensive when evaluated repeatedly, or rely on a multilevel hybridization as proposed in [5]. In practice, for efficiency, the array representing  $g$  is not updated in  $\Omega_{\mathcal{F}}$  and is modified only when a state change occurs.

### 3. MULTISCALE PARAREAL ALGORITHM

In the spirit of [37], we now construct a multiscale parareal algorithm based on the two solvers  $(\mathcal{S}^{\text{HMM}})$  and  $(\mathcal{S}^0)$ .

**3.1. Parallel in time integration.** Let us now recall the parareal algorithm adapted to our multiscale PDE setting. We are interested in the accurate approximation of the macroscopic density  $\rho$  and not on the full kinetic distribution itself. Assuming continuous time, the density  $(\rho(t))_{t \in \mathcal{I}}$  is solution to an ODE of the form

$$\begin{cases} \frac{d}{dt} \rho(t) = \mathcal{S}(\rho), \quad t \in [0, T], \\ \rho(0) = \rho_{\text{in}}, \end{cases}$$

where  $\mathcal{S}$  stands for the numerical methods used. The goal of the parareal algorithm is to approximate the solution at some fixed discrete times  $T^n$ ,

$$\rho^n \approx \rho(T^n), \quad n \in \{0, \dots, N_g\}, \quad N_g \in \mathbb{N}.$$

To do so, instead of using a single time integrator (or propagator), two solvers are coupled through an iterative process: the *parareal iterations*. The first solver is denoted by  $\mathcal{G}(T^n, T^{n+1}, \rho^n)$ . It must be cheap to compute numerically and provides some numerical *guesses* of the behavior of the solution. The second solver, that we denote by  $\mathcal{F}(T^n, T^{n+1}, \rho^n)$ , must be very accurate, and is used to improve the aforementioned guesses.

While the propagator  $\mathcal{G}$  is less costly, its drawback is naturally its precision. However, it is corrected by the accurate, computationally expensive, propagator  $\mathcal{F}$ . The algorithm then unfolds as follows:

- (1) Divide the time domain in  $N_g \in \mathbb{N}$  subintervals  $[T^n, T^{n+1}]$ ,  $n \in \{0, \dots, N_g - 1\}$ ;
- (2) Perform a first coarse guess:

$$\rho^{n+1,0} = \mathcal{G}(T^n, T^{n+1}, \rho^{n,0}) = \rho_{\text{in}};$$

- (3) Refine the guess through the parareal iterations:

$$\rho^{n+1,k+1} = \mathcal{G}(T^n, T^{n+1}, \rho^{n,k+1}) + \mathcal{F}(T^n, T^{n+1}, \rho^{n,k}) - \mathcal{G}(T^n, T^{n+1}, \rho^{n,k}),$$

where  $k = 1, 2, \dots$  denotes the  $k^{\text{th}}$  parareal iteration.

The advantage of this iterative algorithm is its ability to compute the expensive fine propagations in parallel. Therefore, as long as the number of parareal iterations remains small enough to obtain a given accuracy, one can expect a reduction of the computational cost of the time integration.

**3.2. Linking the scales.** A crucial point of multiscale algorithms is about linking the various scales. Thanks to the micro-macro framework, the unknown of the system are now the perturbation at the kinetic level and the density at the fluid one. Consequently, macroscopic data are available at any point in space and any time, without the need of projecting a distribution towards its moments. Nonetheless, one still needs to define a lifting procedure to recover the perturbation. To lift a macroscopic density  $\rho(t, x)$  to a phase-space perturbation, we build upon the Chapman-Enskog expansion (4). The perturbation, that is the unknown of scheme  $(\mathcal{SHMM})$ , can be reconstructed as follows:

**Definition 1.** Let  $L \in \mathbb{N}$ . For a macroscopic quantity  $\rho(t, x)$ , the lifting of order  $L$ , denoted  $\mathcal{L}^L \rho(t, x, v) = g(t, x, v)$ , is defined as

$$\mathcal{L} \rho = g = \sum_{l=1}^L \varepsilon^l h^{(l)},$$

where the perturbations  $h^{(l)}$  depend on velocity moments of  $\mathcal{M}$  and on the derivatives of  $\rho$  and  $E$ .

It is worth mentioning that the mass of the perturbation  $g$  is 0 by construction. More precisely, the zeroth order moment of  $g$  in velocity is 0. This property is of particular importance in the discrete setting to ensure mass conservation in the end. Indeed, the mass is only be supported by the density  $\rho$  in the micro-macro decomposition  $f = \rho \mathcal{M} + g$ .

**3.3. Multiscale algorithm.** Once the parallel in time integration is defined, it can be adapted to the multiscale setting thanks to a discrete counterpart of the lifting operator  $\mathcal{L}$ . Taking advantage of the micro-macro framework, the macroscopic quantity  $\rho$  is always available from  $(\mathcal{SHMM})$  and  $(\mathcal{SMM})$ . It only remains to reconstruct the perturbation  $g$ . For all  $(i, j) \in \mathcal{I} \times \mathcal{J}$ , we define

$$(\mathcal{L} \rho)_{ij} = g_{ij} = \sum_{l=1}^L \varepsilon^l h_{ij}^{(l)}.$$

With this definition, one can actually check that the discrete integral in velocity of such  $g_{ij}$  is 0 and deduce that the discrete perturbation has zero mass. To approximate the perturbations  $h^{(l)}$ , high-order finite differences are used (See Table 1). It is worth mentioning that for  $L = 2$ , the perturbation involves up to fourth order derivatives of the density and third order on the electrical field. In addition, the lifting is defined at cell centers but the scheme  $(\mathcal{SMM})$  requires a perturbation at interfaces. In practice, average interface values of the density can be used in the lifting procedure.

Let us now precise the fine and coarse solvers. We set  $\mathcal{F} = \mathcal{S}^{\text{HMM}}$  the hybrid micro-macro scheme that takes as input a macroscopic density and a perturbation. The coarse solver is set to  $\mathcal{G} = \mathcal{S}^0$  and only depends on the density. The fully multiscale method is summarized in Algorithm 1.

Another crucial point of the method is the computation of the electrical field from the coupling with the Poisson equation. We consider explicit in time discretization and the

electrical field is therefore obtained from the density when needed. In particular, the parareal correction is not applied to the electrical field. The corrected field is computed from the corrected density.

---

**Algorithm 1** Multiscale kinetic parareal Algorithm

---

**Require:**  $\rho^{0,0}$  and  $g^{0,0}$

- 1: Solve for  $E^{0,0}$  using  $\rho^{0,0}$
- 2: **for**  $n = 1, \dots, N_g$  **do** ▷ First coarse guess
- 3:    $\rho^{n,0} \leftarrow \mathcal{S}^0(\rho^{n-1,0})$
- 4:   Solve for  $E^{n,0}$  using  $\rho^{n,0}$
- 5:    $g^{n,0} \leftarrow \mathcal{L}^L(\rho^{n,0})$
- 6: **end for**
- 7: **while**  $k \leq K$  **or** error  $\geq \text{tol}$  **do** ▷ Parareal iterations
- 8:   **for**  $n = k, \dots, N_g$  **do** ▷ Compute density jumps in parallel
- 9:      $\Delta^{n,k} \leftarrow \mathcal{S}^{\text{HMM}}(\rho^{n-1,k}, g^{n-1,k}) - \mathcal{S}^0(\rho^{n-1,k})$
- 10:   **end for**
- 11:   **for**  $n = k, \dots, N_g$  **do** ▷ Sequential correction
- 12:      $\rho^{n,k+1} \leftarrow \mathcal{S}^0(\rho^{n-1,k}) + \Delta^{n,k}$
- 13:     Solve for  $E^{n,k}$  using  $\rho^{n,k}$
- 14:      $g^{n,k+1} \leftarrow \mathcal{L}^L(\rho^{n,k+1})$
- 15:   **end for**
- 16:   Compute successive error  $\max_n \{|\rho^{n,k} - \rho^{n,k-1}|\}$  and  $k \leftarrow k + 1$
- 17: **end while**

---

**Lemma 1** (Conservation of mass). *Let  $(\rho_i^{n,k})_{(n,i) \in \mathcal{I} \times \{0, \dots, N_g\}}$  be given by Algorithm 1 and assume exact mass conservation of the hybrid numerical method  $(\mathcal{S}^{\text{HMM}})$ . We denote the mass of the system at time  $t^n$  and parareal iteration  $k$  as*

$$m^{n,k} = \sum_{i \in \mathcal{I}} \rho_i^{n,k} \Delta x. \quad (9)$$

Then, for all  $k > 0$  and all  $n \in \{0, \dots, N_g\}$ ,

$$m^{n,k+1} = m^{0,0}. \quad (10)$$

*Proof.* A first observation is that, by construction of the parareal algorithm, for all  $k \geq 0$ ,

$$m^{0,k} = m^{0,0}, \quad (11)$$

since the initial data is fixed. Then, let  $n \in \{0, \dots, N_g\}$  and let  $(\rho_i^n)_{i \in \mathcal{I}}$  be given by Algorithm 1. By construction of the asymptotic scheme  $(\mathcal{S}^0)$  and the assumption on the hybrid method  $(\mathcal{S}^{\text{HMM}})$  one has the following properties:

$$\sum_{i \in \mathcal{I}} \mathcal{S}^0(\rho^{n,k})_i \Delta x = m^{n,k}, \text{ and } \sum_{i \in \mathcal{I}} \mathcal{S}^{\text{HMM}}(\rho^{n,k})_i \Delta x = m^{n,k}. \quad (12)$$

In addition, updating the perturbation with  $(\mathcal{S}^{\text{MM}})$  preserves its 0 mass by construction. This property carries over under the action of the hybrid scheme  $(\mathcal{S}^{\text{HMM}})$  as this property only depends on the velocity variable and not on the spatial coupling. Using the update relation of the parareal algorithm, one has:

$$m^{n,k+1} = \sum_{i \in \mathcal{I}} \mathcal{S}^0(\rho^{n-1,k+1})_i \Delta x + \sum_{i \in \mathcal{I}} \mathcal{S}^{\text{HMM}}(\rho^{n-1,k-1})_i \Delta x - \sum_{i \in \mathcal{I}} \mathcal{S}^0(\rho^{n-1,k-1})_i \Delta x \quad (13)$$

Thanks to (12), it follows that for all  $k \geq 0$

$$m^{n,k+1} = m^{n-1,k+1} \quad (14)$$

One then obtains (10) by induction over  $n$ , using (11). □

# CPUs	Intel(R) Xeon(R) Platinum 8268 CPU @ 2.90GHz x2
# cores	48
RAM	750 GB

TABLE 2. Computing architecture.

**Remark 1.** As pointed out in [34], the hybrid method  $(\mathcal{S}^{\text{HMM}})$  is not exactly conservative. However, the mass variation is in practice negligible for reasonable coupling thresholds. In addition, the exact mass variation decays very fast as  $\varepsilon \rightarrow 0$  (See Lemma 4.2 in [34]). Exact mass conservation could be achieved using, for example, different boundary conditions between kinetic and fluid states following the approaches in [23, 5] by matching fluxes.

#### 4. IMPLEMENTATION

The computational gain of Algorithm 1 compared to the standard AP scheme  $(\mathcal{S}^{\text{MM}})$  depends on two main factors. First, parallelization allows the computational load of the kinetic propagations that are needed to compute the correction, to be distributed efficiently. Second, the implementation of dynamic domain adaptation accelerates computations independently of parallel resources, providing speed-ups even without multiple processors, unlike the parareal algorithm.

Algorithm 1 is currently implemented in Fortran08 using a shared-memory framework with OpenMP. To minimize overhead from memory allocations and deallocations, arrays required for the hybrid propagation, that are executed in parallel, are preallocated per thread. In a distributed-memory framework, these considerations are replaced by communication management. Moreover, since the workload of the parallel loop can vary significantly depending on proximity to equilibrium, a dynamic scheduling was found to offer the best performance, despite the small additional overhead.

Assuming the cost of communications is negligible compared to the solver times — which is reasonable in our shared-memory framework — we denote by  $T_{\text{HMM}}$  (resp.  $T_{\text{Fluid}}$ ) the maximum time for  $(\mathcal{S}^{\text{HMM}})$  (resp.  $(\mathcal{S}^0)$ ) to evolve a given initial data from  $T^n$  to  $T^{n+1}$ . The maximum is taken over all propagations because, on each sub-time interval, the stability conditions and the domain adaptation may vary. In addition, the cost of the lifting operator, which is fully non-local in both position (due to derivative computations) and velocity, can be significant; we denote this cost by  $T_{\text{Lift}}$ . The ideal numerical cost of Algorithm 1 on  $N_p$  threads with  $N_g$  sub-time intervals is then given by the formula:

$$T_{\text{Parareal}} = T_{\text{Fluid}} + N_g k \left( \frac{T_{\text{Lift}} + T_{\text{HMM}} + T_{\text{Fluid}}}{N_p} + T_{\text{Fluid}} \right).$$

Consequently, the ideal number of parareal iterations to be less costly than a fully kinetic simulation should satisfy:

$$T_{\text{Parareal}} \leq N_g T_{\text{HMM}}$$

or stated differently,

$$k_{\text{opt}} \leq \left\lceil \frac{N_g T_{\text{HMM}} - T_{\text{Fluid}}}{N_g \left( \frac{T_{\text{Lift}} + T_{\text{HMM}} + T_{\text{Fluid}}}{N_p} + T_{\text{Fluid}} \right)} \right\rceil.$$

The performance of the multiscale algorithm was evaluated on the architecture presented in Table 2.

#### 5. NUMERICAL RESULTS

For practical purposes, the velocity domain is truncated to the box  $[-v_*, v_*]$ , and we denote by  $x_*$  the length of the 1-dimensional torus  $\mathbb{T}$ . Unless stated otherwise, the discretization parameters are fixed as

$$N_x = 32, \quad N_{v_x} = 32, \quad N_{v_y} = N_{v_z} = 16, \quad x_* = 2\pi, \quad v_* = 8.$$

We consider the following far-from-equilibrium initial condition:

$$f(0, x, v) = \mathcal{M}(v_x, v_y, v_z), v_x^4 \left( 1 + 0.9 \cos \left( \frac{2\pi x}{x_*} \right) \right).$$

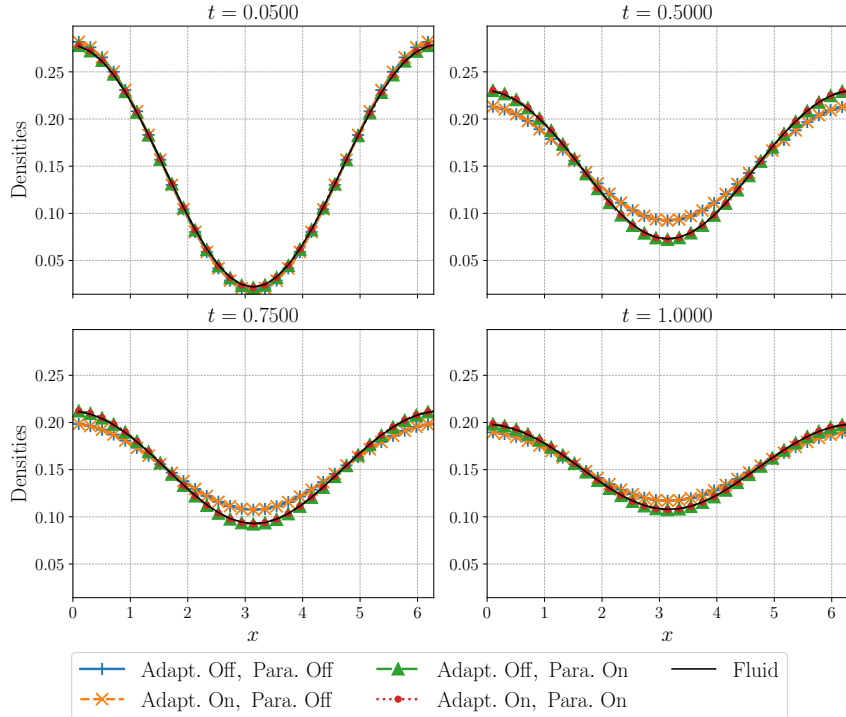


FIGURE 2. Density snapshots for  $\varepsilon = 0.5$  obtained with Algorithm 1.

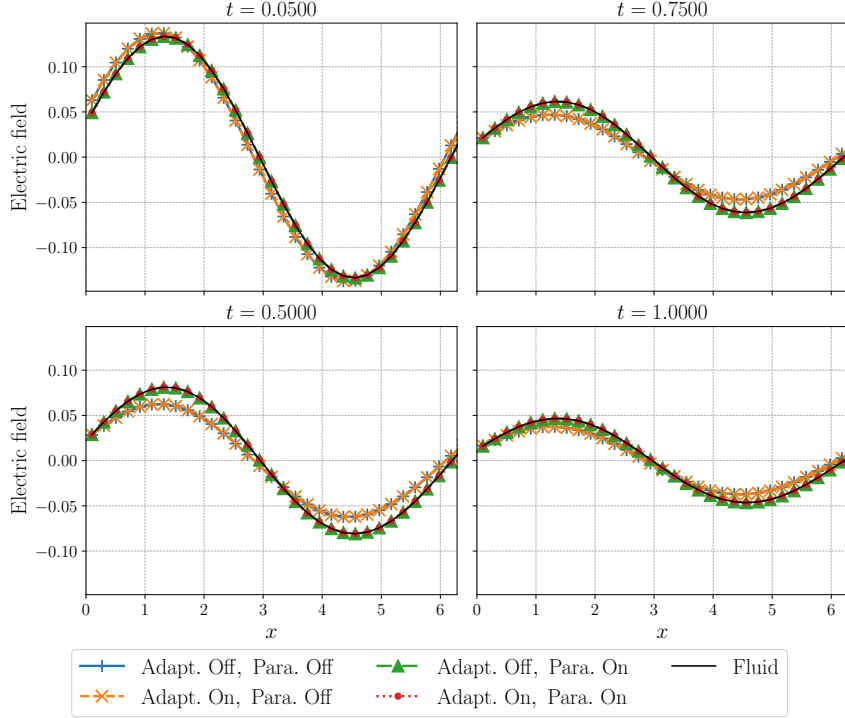
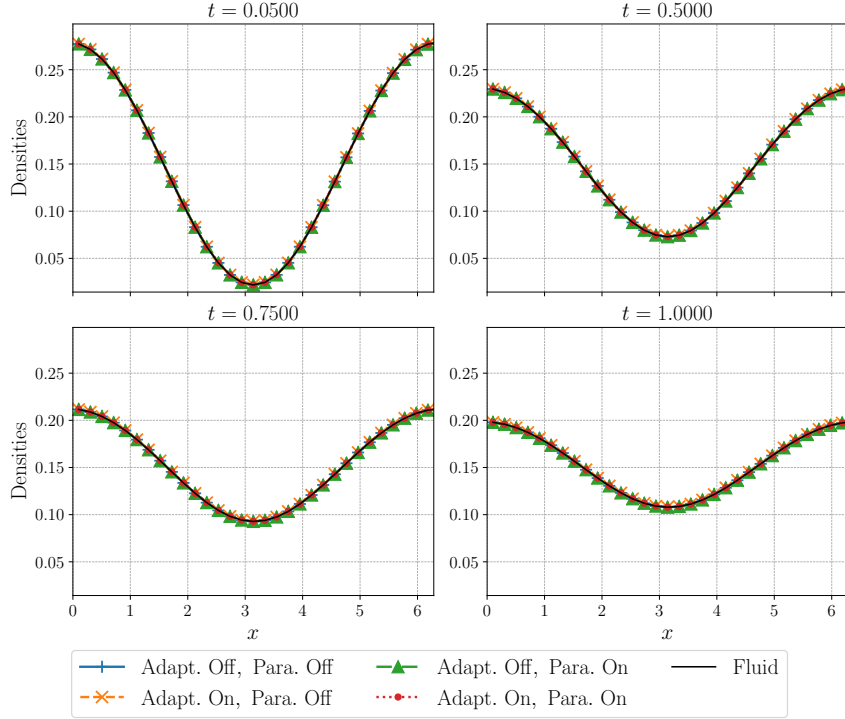
The thresholds for the dynamic domain adaptation indicators are set to  $\eta_0 = \delta_0 = 10^{-5}$ . These empirical values are an order of magnitude lower than the ones used in [34] where their impact and accuracy was investigated. These thresholds are chosen as a good compromise between accuracy and acceleration. The perturbation  $g$  is reconstructed at order  $L = 2$ , which provides the most accurate results compared to lower-order reconstructions and is consistent with the derivation of the macroscopic indicators.

The number of coarse time intervals is set to  $N_g = 200$ . This value guarantees convergence across all regimes. While regimes with  $\varepsilon \ll 1$  require relatively few coarse intervals, it was observed that in the kinetic, transport-dominated regime ( $\varepsilon \sim 1$ ), convergence is slower, and a larger value of  $N_g$  is necessary.

Figures 2 and 3 shows snapshots of the densities and electric field computed with Algorithm 1 for  $\varepsilon = 0.5$ , with and without activation of the multiscale procedures (parareal integration and domain adaptation). The corresponding results for  $\varepsilon = 10^{-4}$  are shown in Figures 4 and 5. In both the kinetic regime ( $\varepsilon = 0.5$ ) and the fluid regime ( $\varepsilon = 10^{-4}$ ), the different methods agree closely. Furthermore, the asymptotic-preserving property is confirmed, as the hybrid solutions all coincide with the limiting fluid solution for small  $\varepsilon$ .

**5.1. Convergence.** We investigate the convergence of Algorithm 1. Figure 6 shows the evolution of the error between two consecutive parareal iterations, for  $\varepsilon \in [10^{-7}, 1]$  with and without domain adaptation, at final time  $T_f = 1.0$ . The algorithm converges up to machine accuracy in all cases, with iteration counts strongly dependent on  $\varepsilon$ : fewer than five iterations suffice for small  $\varepsilon$ , while about twenty are required when  $\varepsilon \sim 1$ . This behavior reflects that, as  $\varepsilon \rightarrow 0$ , the fluid predictor provides a more accurate description of the system. Since the limiting system is parabolic, convergence is further improved, consistent with the known difficulty of the parareal method in transport-dominated regimes.

Dynamic domain adaptation further accelerates convergence. Once activated, the predictor coincides with the fine correction, reducing the number of parareal iterations. This improvement must be weighed against the computational trade-offs of looser coupling thresholds and the accuracy loss inherent in adopting the fluid approximation.

FIGURE 3. Electric field snapshots for  $\varepsilon = 0.5$  obtained with Algorithm 1.FIGURE 4. Density snapshots for  $\varepsilon = 10^{-4}$  obtained with Algorithm 1.

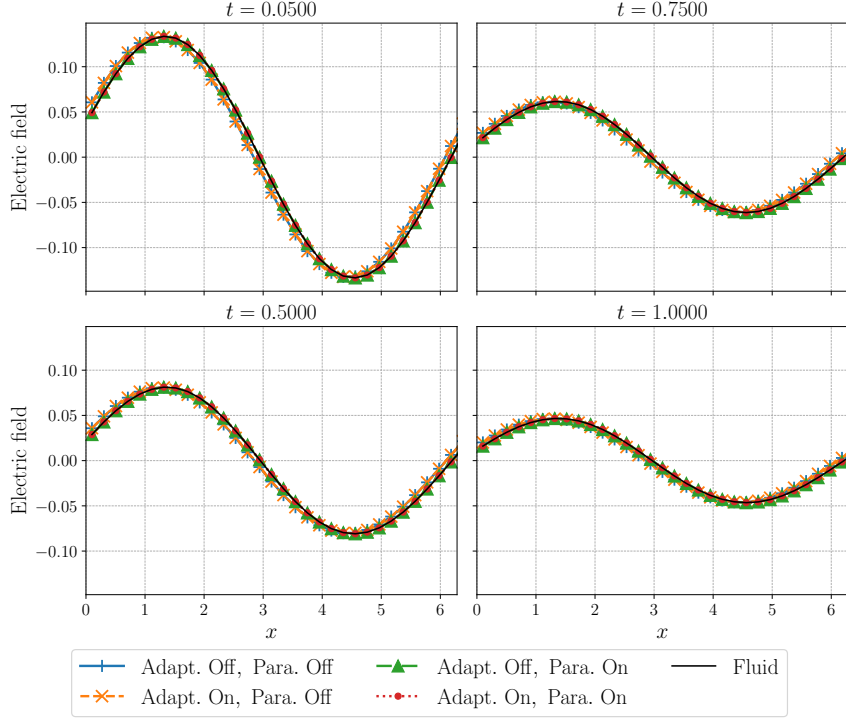
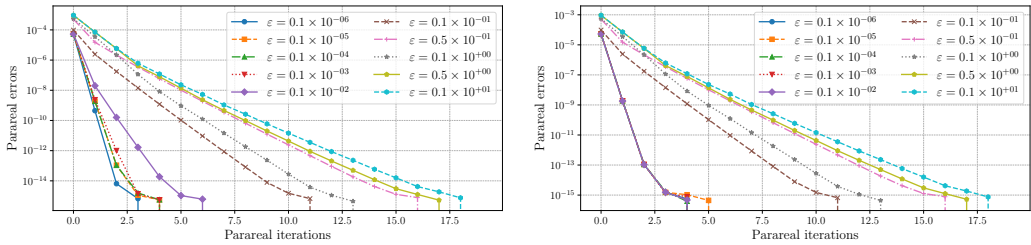
FIGURE 5. Electric field snapshots for  $\varepsilon = 10^{-4}$  obtained with Algorithm 1.FIGURE 6. Convergence of Algorithm 1 for different values of  $\varepsilon$ : without domain adaptation (left) and with domain adaptation (right).

Figure 7 reports the  $L^\infty$  error over time between the classical approximation (without parareal integration or domain adaptation) and the multiscale methods. Without parareal integration, the error remains small, since domain adaptation is only triggered in fluid regions where it provides a good approximation. With parareal integration, a maximum error of order  $10^{-2}$  is observed in the kinetic regime  $\varepsilon = 0.5$ , reflecting that the fluid predictor is too crude and even a second-order reconstruction of the perturbation cannot fully compensate. Nevertheless, second-order reconstruction yields the smallest error compared to lower-order variants. In the fluid regime  $\varepsilon = 10^{-4}$ , the error relative to the classical scheme drops to about  $10^{-5}$ . Finally, as the long-time behavior of  $(\mathcal{P}^\varepsilon)$  is relaxation to a constant state determined by the torus length and the initial mass [16], the error naturally vanishes as  $t \rightarrow \infty$ . It should be noted that the errors in Figure 7 are of a different nature from those in Figure 6. The latter illustrates the convergence of Algorithm 1, without indicating the solution it converges to. A detailed analysis of this aspect lies beyond the scope of this work and would require a careful study of the multiscale operators' properties, as performed in [46].

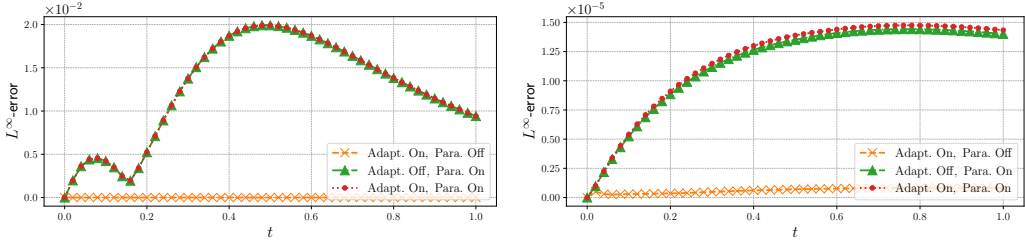


FIGURE 7.  $L^\infty$ -error of Algorithm 1 with respect to the classical scheme without parareal integration or domain adaptation, for  $\varepsilon = 0.5$  (left) and  $\varepsilon = 10^{-4}$  (right).

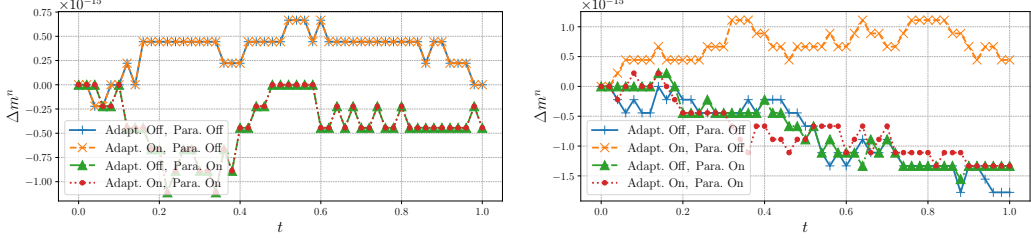


FIGURE 8. Mass variation for Algorithm 1 with  $\varepsilon = 0.5$  (left) and  $\varepsilon = 10^{-4}$  (right).

**5.2. Performances.** To assess the performance of the fully hybrid method, we set  $N_x = 32$ ,  $N_{v_x} = 32$ ,  $N_{v_y} = N_{v_z} = 16$  and  $N_g = 200$ . In addition, the error threshold in the parareal algorithm is set to  $10^{-10}$  and the coupling parameters are again set to  $\eta_0 = \delta_0 = 10^{-5}$ . The number of OpenMP threads is fixed to 48 on the architecture described in Table 2. The corresponding runtimes and speedups are reported in Table 3.

The results show that Algorithm 1 consistently outperforms the standard kinetic scheme for all values of  $\varepsilon$ . This demonstrates the ability of the multiscale method to exploit parallel-in-time acceleration in kinetic regimes while benefiting from domain adaptation in transient and near-fluid regimes. Moreover, the method remains stable across the full range of  $\varepsilon$ , confirming its AP property.

Without domain adaptation, for  $\varepsilon = 1$  we observe a speedup of about 2, which increases to 3 at  $\varepsilon = 10^{-2}$  and 7 at  $\varepsilon = 10^{-4}$ . This first shows that the multiscale parareal algorithm applied to  $(\mathcal{P}^\varepsilon)$  can already reduce the computational cost of the time integration.

Enabling the domain adaptation, which mainly occurs in near-fluid regimes or in long time [34], one observes that it indeed helps to further reduce the computational time with a speedup factor that reaches up to 73 at  $\varepsilon = 10^{-4}$ . In the case  $\varepsilon = 10^{-3}$  (italicized values), a numerical interplay was observed between the two hybrid methods, and Algorithm 1 converged only to a successive error of  $10^{-5}$ , after five iterations. The runtime corresponding to these five iterations was used to compute the speedup.

Several remarks must be made regarding the performance of the algorithm. First, even with a relatively small number of grid points in each variable, significant speedups are already observed. These would naturally become even more significant as the cost of the kinetic solver increases drastically by refining the mesh. Secondly, the performance of the domain adaptation is directly related to the coupling thresholds  $\eta_0$  and  $\delta_0$  that are currently chosen empirically.

**5.3. Mass conservation.** A key feature of  $(\mathcal{P}^\varepsilon)$  is the conservation of moments. In the linear relaxation case, only the mass is conserved. Figure 8 reports the evolution of the mass variation

$$\Delta m^n = \sum_{i \in \mathcal{I}} (\rho_i^n - \rho_i^0) \Delta x. \quad (15)$$

Consistently with Lemma 1, Algorithm 1 preserves mass up to machine precision, independently of the activation of the dynamic domain adaptation.

$\varepsilon$	Runtimes (s)				Fluid	
	Para. Off		Para. On			
	Adapt. Off	Adapt. On	Adapt. Off	Adapt. On		
1.0	96.1 <b>1.00</b>	104.6 <b>0.92</b>	42.38 <b>2.27</b>	44.5 <b>2.16</b>	0.25 <b>384</b>	
$10^{-1}$	96.1 <b>1.00</b>	104.2 <b>0.92</b>	35.2 <b>2.73</b>	37.5 <b>2.56</b>	0.25 <b>384</b>	
$10^{-2}$	96.1 <b>1.00</b>	99.5 <b>0.97</b>	31.1 <b>3.09</b>	32.5 <b>2.96</b>	0.25 <b>384</b>	
$10^{-3}$	96.1 <b>1.00</b>	20.6 <b>4.67</b>	17.0 <b>5.65</b>	4.0 <b>24.02</b>	0.25 <b>384</b>	
$10^{-4}$	96.1 <b>1.00</b>	0.19 <b>506</b>	13.0 <b>7.39</b>	1.32 <b>72.80</b>	0.25 <b>384</b>	

TABLE 3. Runtimes and speedups of Algorithm 1 for different  $\varepsilon$ .

## 6. CONCLUSION

In this work we have presented a fully multiscale method for kinetic equations. The approach combines the advantages of AP schemes, dynamic domain adaptation, and parallel-in-time integration, leading to a significant reduction in numerical cost across all regimes of the scaling parameters. Apart from minimal numerical thresholds, the method accelerates computations automatically, without requiring user intervention or solver selection.

In addition, even larger computational gains can be expected in more complex settings, such as higher-dimensional problems in physical space, boundary conditions, or Boltzmann-type collision operators that significantly increase the cost of kinetic solvers, enhancing the need for accelerating methods.

The current implementation relies on a shared-memory framework. Possible extensions include implementing the method to distributed-memory architectures and parallelizing the hybrid solvers within the parareal algorithm. The method appears promising to extend towards more physically relevant models such as two species systems appearing in semiconductor modelling or plasma physics.

## ACKNOWLEDGEMENT

The author would like to thank T. Rey and the Université Côte d’Azur for the computing resources used in this work.

The author has received funding from the European Research Council (ERC) under the European Union’s Horizon 2020 research and innovation program (grant agreement No 865711).

## REFERENCES

- [1] ABDULLE, A., E, W., ENGQUIST, B., AND VANDEN-EIJNDEN, E. The heterogeneous multiscale method. *Acta Numer.* 21 (2012), 1–87.
- [2] ANGEL, J., GÖTSCHEL, S., AND RUPRECHT, D. Impact of spatial coarsening on parareal convergence. Preprint arXiv:2111.10228, 2021.
- [3] BAL, G. On the convergence and the stability of the parareal algorithm to solve partial differential equations. In *Domain decomposition methods in science and engineering. XV. Selected papers of the 15th international conference on domain decomposition, Berlin, Germany, July 21–25, 2003*. Berlin: Springer, 2005, pp. 425–432.
- [4] BOSSUYT, I., VANDEWALLE, S., AND SAMAÉY, G. Monte-Carlo/Moments micro-macro Parareal method for unimodal and bimodal scalar McKean-Vlasov SDEs. Preprint arXiv:2310.11365, 2023.
- [5] CAPARELLO, D., PARESCHI, L., AND REY, T. Hierarchical dynamic domain decomposition for the multiscale Boltzmann equation. Preprint, arXiv:2505.03360, 2025.

- [6] CRESTETTO, A., CROUSEILLES, N., DIMARCO, G., AND LEMOU, M. Asymptotically complexity diminishing schemes (ACDS) for kinetic equations in the diffusive scaling. *J. Comput. Phys.* 394 (2019), 243–262.
- [7] CROUSEILLES, N., AND LEMOU, M. An asymptotic preserving scheme based on a micro-macro decomposition for collisional Vlasov equations: diffusion and high-field scaling limits. *Kinet. Relat. Models* 4, 2 (2011), 441–477.
- [8] DE STERCK, H., FALGOUT, R. D., AND KRZYSIK, O. A. Fast multigrid reduction-in-time for advection via modified semi-Lagrangian coarse-grid operators. *SIAM J. Sci. Comput.* 45, 4 (2023), a1890–a1916.
- [9] DEGOND, P., DIMARCO, G., AND MIEUSSENS, L. A moving interface method for dynamic kinetic-fluid coupling. *J. Comput. Phys.* 227, 2 (2007), 1176–1208.
- [10] DEGOND, P., GOUDON, T., AND POUPAUD, F. Diffusion limit for non homogeneous and non-micro-reversible processes. *Indiana Univ. Math. J.* 49, 3 (2000), 1175–1198.
- [11] DEGOND, P., JIN, S., AND MIEUSSENS, L. A smooth transition model between kinetic and hydrodynamic equations. *J. Comput. Phys.* 209, 2 (2005), 665–694.
- [12] DIMARCO, G., MIEUSSENS, L., AND RISPOLI, V. An asymptotic preserving automatic domain decomposition method for the Vlasov-Poisson-BGK system with applications to plasmas. *J. Comput. Phys.* 274 (2014), 122–139.
- [13] DIMARCO, G., AND PARESCHI, L. Hybrid multiscale methods. II: Kinetic equations. *Multiscale Model. Simul.* 6, 4 (2008), 1169–1197.
- [14] DIMARCO, G., AND PARESCHI, L. Numerical methods for kinetic equations. *Acta Numer.* 23 (2014), 369–520.
- [15] DOBREV, V. A., KOLEV, T., PETERSSON, N. A., AND SCHRODER, J. B. Two-level convergence theory for multigrid reduction in time (MGRIT). *SIAM J. Sci. Comput.* 39, 5 (2017), s501–s527.
- [16] DOLBEAULT, J., MOUHOT, C., AND SCHMEISER, C. Hypocoercivity for linear kinetic equations conserving mass. *Trans. Am. Math. Soc.* 367, 6 (2015), 3807–3828.
- [17] DUARTE, M., MASSOT, M., AND DESCUMBES, S. Parareal operator splitting techniques for multi-scale reaction waves: numerical analysis and strategies. *ESAIM, Math. Model. Numer. Anal.* 45, 5 (2011), 825–852.
- [18] E, W. *Principles of Multiscale Modeling*. Cambridge University Press, Cambridge, 2011.
- [19] E, W., AND ENGQUIST, B. The Heterogeneous Multiscale Methods. *Commun. Math. Sci.* 1, 1 (2003), 87 – 132.
- [20] EGHBAL, A., GERBER, A. G., AND AUBANEL, E. Acceleration of unsteady hydrodynamic simulations using the parareal algorithm. *J. Comput. Sci.* 19 (2017), 57–76.
- [21] FALGOUT, R. D., FRIEDHOFF, S., KOLEV, T. V., MACLACHLAN, S. P., AND SCHRODER, J. B. Parallel time integration with multigrid. *SIAM J. Sci. Comput.* 36, 6 (2014), c635–c661.
- [22] FARHAT, C., AND CHANDESRIS, M. Time-decomposed parallel time-integrators: Theory and feasibility studies for fluid, structure, and fluid-structure applications. *Int. J. Numer. Methods Eng.* 58, 9 (2003), 1397–1434.
- [23] FILBET, F., AND REY, T. A hierarchy of hybrid numerical methods for multi-scale kinetic equations. *SIAM J. Sci. Comput.* 37, 3 (May 2015), A1218–A1247.
- [24] FILBET, F., AND XIONG, T. A hybrid discontinuous Galerkin scheme for multi-scale kinetic equations. *J. Comput. Phys.* 372 (2018), 841–863.
- [25] GANDER, M. J. Analysis of the parareal algorithm applied to hyperbolic problems using characteristics. *Bol. Soc. Esp. Mat. Apl. SéMA* 42 (2008), 21–35.
- [26] GRIGORI, L., HIRSTOAGA, S. A., AND SALOMON, J. A parareal algorithm for a highly oscillating Vlasov-Poisson system with reduced models for the coarse solving. *Comput. Math. Appl.* 130 (2023), 137–148.
- [27] HESSENTHALER, A., SOUTHWORTH, B. S., NORDSLETTEN, D., RÖHRLE, O., FALGOUT, R. D., AND SCHRODER, J. B. Multilevel convergence analysis of multigrid-reduction-in-time. *SIAM J. Sci. Comput.* 42, 2 (2020), a771–a796.
- [28] HORSTEN, N., SAMAËY, G., AND BAELEMANS, M. A hybrid fluid-kinetic model for hydrogenic atoms in the plasma edge of tokamaks based on a micro-macro decomposition of the kinetic equation. *J. Comput. Phys.* 409 (2020), 23. Id/No 109308.
- [29] HORSTEN, N., SAMAËY, G., AND BAELEMANS, M. A hybrid fluid-kinetic model for hydrogenic atoms in the plasma edge of tokamaks based on a micro-macro decomposition of the kinetic equation. *J. Comput. Phys.* 409 (2020), 109308.
- [30] JIN, S. Efficient asymptotic-preserving (AP) schemes for some multiscale kinetic equations. *SIAM J. Sci. Comput.* 21, 2 (1999), 441–454.
- [31] JIN, S. Asymptotic-preserving schemes for multiscale physical problems. *Acta Numer.* 31 (2022), 415–489.
- [32] KLAR, A. A numerical method for kinetic semiconductor equations in the drift-diffusion limit. *SIAM J. Sci. Comput.* 20, 5 (1999), 1696–1712.
- [33] KOLOBOV, V. I., ARSLANBEKOV, R. R., ARISTOV, V. V., FROLOVA, A. A., AND ZABELOK, S. A. Unified solver for rarefied and continuum flows with adaptive mesh and algorithm refinement. *J. Comput. Phys.* 223, 2 (2007), 589–608.
- [34] LAIDIN, T. Hybrid kinetic/fluid numerical method for the Vlasov-BGK equation in the diffusive scaling. *Kinet. Relat. Mod.* (2023).
- [35] LAIDIN, T. *Méthodes numériques hybrides cinétique/fluide et préservant la structure pour des équations cinétiques collisionnelles*. Theses, Université de Lille, Sept. 2024.

- [36] LAIDIN, T., AND REY, T. Hybrid kinetic/fluid numerical method for the Vlasov-Poisson-BGK equation in the diffusive scaling. In *Finite volumes for complex applications X – Volume 2. Hyperbolic and related problems. FVCA10, Strasbourg, France, October 30 – November 3, 2023*. Cham: Springer, 2023, pp. 229–237.
- [37] LAIDIN, T., AND REY, T. A Parareal in time numerical method for the collisional Vlasov equation in the hyperbolic scaling. Preprint arXiv:2502.02704, 2025.
- [38] LEGOLL, F., LELIÈVRE, T., AND SAMAEY, G. A micro-macro parareal algorithm: application to singularly perturbed ordinary differential equations. *SIAM J. Sci. Comput.* 35, 4 (2013), a1951–a1986.
- [39] LEMOU, M. Relaxed micro-macro schemes for kinetic equations. *C. R. Acad. Sci. Paris, Ser. I* 348, 7-8 (apr 2010), 455–460.
- [40] LEMOU, M., AND MIEUSSENS, L. A new asymptotic preserving scheme based on micro-macro formulation for linear kinetic equations in the diffusion limit. *SIAM J. Sci. Comput.* 31, 1 (2008), 334–368.
- [41] LEVERMORE, C. D., MOROKOFF, W. J., AND NADIGA, B. T. Moment realizability and the validity of the Navier-Stokes equations for rarefied gas dynamics. *Phys. Fluids* 10, 12 (1998), 3214–3226.
- [42] LIONS, J.-L., MADAY, Y., AND TURINICI, G. A “parareal” in time discretization of PDE’s. *C. R. Acad. Sci. Paris, Sér. I, Math.* 332, 7 (2001), 661–668.
- [43] MADAY, Y., AND TURINICI, G. A parareal in time procedure for the control of partial differential equations. *C. R. Math. Acad. Sci. Paris* 335, 4 (2002), 387–392.
- [44] MARTIN J., G., MARIO, O., AND STEPHAN, R. A parareal algorithm without coarse propagator ? Preprint arXiv : 2409.02673v1, 2024.
- [45] NIELSEN, A. S., BRUNNER, G., AND HESTHAVEN, J. S. Communication-aware adaptive parareal with application to a nonlinear hyperbolic system of partial differential equations. *J. Comput. Phys.* 371 (2018), 483–505.
- [46] SAMAEY, G., AND SLAWIG, T. A micro/macro parallel-in-time (parareal) algorithm applied to a climate model with discontinuous non-monotone coefficients and oscillatory forcing. Preprint arXiv:1806.04442, 2023.
- [47] SUGIYAMA, M., SCHRODER, J. B., SOUTHWORTH, B. S., AND FRIEDHOFF, S. Weighted relaxation for multigrid reduction in time. *Numer. Linear Algebra Appl.* 30, 1 (2023), e2465, 20.
- [48] TIWARI, S. Coupling of the Boltzmann and Euler equations with automatic domain decomposition. *J. Comput. Phys.* 144, 2 (1998), 710–726.
- [49] TIWARI, S. Application of moment realizability criteria for the coupling of the Boltzmann and Euler equations. *Transp. Theory Stat. Phys.* 29, 7 (2000), 759–783.
- [50] TIWARI, S., AND KLAR, A. An adaptive domain decomposition procedure for Boltzmann and Euler equations. *J. Comput. Appl. Math.* 90, 2 (1998), 223–237.